Improvement in the Quality of Flow Visualization in the Langley 0.3-Meter Transonic Cryogenic Tunnel

Walter L. Snow, Alpheus W. Burner, and William K. Goad

AUGUST 1986

NASA

Improvement in the Quality of Flow Visualization in the Langley 0.3-Meter Transonic Cryogenic Tunnel

Walter L. Snow, Alpheus W. Burner, and William K. Goad

Langley Research Center
Hampton, Virginia

Introduction

Cryogenic wind tunnels exploit the temperature dependence of viscosity in conjunction with high pressure to achieve full-scale Reynolds numbers. The unique characteristics of such facilities are detailed in reference 1. The extreme temperature excursions encountered in these tunnels pose challenging problems for instrumentation. This report deals with difficulties encountered when implementing optical diagnostic techniques in a small cryogenic wind tunnel. Reference 2 noted a graininess and jumbling of fringes in holographically recorded interferograms under conditions of low temperature and high pressure. Reference 3 describes similar degradation of optical quality for conventional imaging, the modulation transfer function being used to quantify the losses. Researchers experimenting with white light schlieren, shadowgraph, and moirè deflectometry measurements in this facility have also noted the reduced quality. (See ref. 4.) In references 2 and 3 the reduced quality in flow visualization was attributed to effects originating in the test section. This conclusion has since been shown to be erroneous.

Symbols

f	focal length, cm
K	Gladstone-Dale constant, cm^3/g
M	gram molecular weight, g/mole
n	refractive index
$n_{2,1}$	relative index of refraction, n_2/n_1
p	pressure, atm (1 atm = 101.325 kPa)
r	radius of gas bubble, cm
R	universal gas constant, 82.082 cm^3-atm/deg-mole
T	temperature, K
w	measured width of slit image, mm
w_{ref}	width of slit image measured under ambient conditions
ρ	mass density, g/cm^3

Subscripts:

1	surrounding medium
2	gas bubble
t	total

Test Facility

The Langley 0.3-Meter Transonic Cryogenic Tunnel (0.3-m TCT) is a continuous-flow, fan-driven tunnel which uses nitrogen as a test gas and is cooled by injecting liquid nitrogen directly into the stream. The total temperature T_t in the 0.3-m TCT can range from 80 to 330 K while the total pressure p_t can be varied from 1.2 to 6.0 atm (1 atm = 101.325 kPa). Reynolds numbers of over 330×10^6 per meter are attainable in this facility. Some of the design features and operational characteristics of the 0.3-m TCT have been reported in reference 5. A schematic of the 0.3-m TCT circuit is shown in figure 1.

A top view of the plenum and test section area with cover removed is provided in figure 2 to show the slotted floor and the windows located in the model support turntables. The windows used for flow visualization are schlieren quality fused silica. Special D-shaped windows are required when the model turntable is installed as detailed in references 2 and 3. The outer pressure shell can accommodate up to 23-cm (9-in.) diameter windows. For this study, inserts were provided for 7.6-cm (3-in.) diameter ports. With the outer windows in place, equipment pods are attached to either or both sides of the tunnel. The pods are used primarily as test stands for optical experiments concerning the flow field.

Figure 3 is a schematic drawing showing the relationship of the pods to the wind tunnel with a typical schlieren configuration installed. The light source is a 75-watt xenon arc lamp. A condenser lens focuses the light source onto a 0.51-mm (20-mil) diameter pinhole. Light folded with a 10-cm diameter flat mirror is collimated with an $f/8$ mirror with a 1.22-m (48-in.) focal length. The source can be operated either in a continuous mode or in 10-microsecond single or repetitive flash mode. Several variations of this setup were used to evaluate the optical quality of the flow field without a model in the test section.

Pressure and Temperature Effects on Refractive Index

Interaction of a light beam with matter may alter some characteristics of the light such as phase, polarization, and intensity. These alterations constitute the basis for optical diagnostic techniques. Effects along the path length are cumulative, and attempts to infer the location of the effects from knowledge of input and output fields are generally intractable in the absence of auxiliary information or assumptions. In the case of conventional schlieren techniques, for example, quality optics are used to generate and maintain well-defined wave fronts. Any perturbations to the beam are assumed to occur only

in the region of interest. Consequently, windows or optical elements that compromise the wave front by altering its phase affect the results. Turbulence-induced irregularities in the refractive index also distort the optical wave fronts. As radiation with a distorted wave front propagates, its local irradiance varies because of the focusing and spreading effects of the front, with image motion, distortion, and blurring resulting. The subject of light beam propagation through turbulent media is introduced in references 6 and 7 and is an area of active research.

A medium is characterized optically by the refractive index, which is directly proportional to density in the absence of nonlinearities induced by intense electric fields. In particular,

$$n - 1 = K\rho \qquad (1)$$

where K is the Gladstone-Dale constant ($0.238\,\text{cm}^3/\text{g}$ for nitrogen) and ρ is the mass density. For an ideal gas,

$$\rho = \frac{Mp}{RT} \qquad (2)$$

where R is the universal gas constant, and M is the gram molecular weight (28.02 grams for molecular nitrogen). From equations (1) and (2),

$$dn = K\,d\rho = \frac{MK\,dp}{RT} - \frac{MKp\,dT}{RT^2} \qquad (3)$$

Generally, turbulence-induced pressure variations are negligible compared with temperature-induced variations. For propagation of beams in the atmosphere, one frequently encounters (ref. 8)

$$\frac{dn}{dT} = \frac{78p}{T^2} \times 10^{-6} \qquad [\text{K}^{-1}]$$

where p is the local pressure in millibars, and T is the absolute Kelvin temperature. This expression is responsible for the convenient rule of thumb that $dn/dT = 10^{-6}\,\text{K}^{-1}$ at standard temperature and pressure. High-pressure, cryogenic conditions increase the temperature sensitivity by one or two orders of magnitude. Optical beams are especially vulnerable in regions of high temperature gradients since natural or forced convection can easily mix parcels of gas having temperature differences.

Consider the optical power of a gas "lens" in the form of a spherical bubble having density ρ_2 entrained in a gas of density ρ_1. If the radius of the bubble is r, then its focal length can be computed using the thick lens formula

$$\frac{1}{f} = (n_{2,1} - 1)\frac{2}{r} - \frac{(n_{2,1} - 1)^2}{n_{2,1}}\frac{2}{r} = \frac{2(n_{2,1} - 1)}{rn_{2,1}} \qquad (4)$$

where $n_{2,1}$ is the relative refractive index of the bubble with respect to the surrounding gas. Equations (1) and (2) can be used to write the expression in terms of thermodynamic variables as

$$\frac{1}{f} = \frac{2}{r}\frac{K(\rho_2 - \rho_1)}{(1 + K\rho_2)} = \frac{2}{r}\frac{KMp}{(RT_2 + KMp)}\frac{(T_1 - T_2)}{T_1} \qquad (5)$$

Let $\Delta T = T_2 - T_1$ and note that

$$RT_2 + KMp = RT_1 + R\,\Delta T + KMp \approx RT_1$$

Then with the subscript on T dropped, equation (5) becomes

$$\frac{1}{f} \approx \frac{2}{r}\frac{KM}{R}\frac{p\,\Delta T}{T^2} \qquad (6)$$

This equation explicitly displays the p/T^2 dependence of the focusing power of a bubble of gas differing in the temperature by ΔT from its environment.

Evolution of Tests Pertaining to Flow Visualization Quality

Holographic Interferometry

Reference 2 describes initial attempts to apply holographic interferometry in the 0.3-m TCT. The optical layout is depicted in figure 4(a). The quality of flow visualization obtained in this series of tests degraded with increasing pressure and especially with decreasing temperature. To obtain an index of the degradation, the spot size of the focus point of the reconstructed holographic field was measured. The measured spot size is plotted as a function of $1/T_t$ and p_t/T_t^2 in accord with equation (3) with results as shown in figure 4. The high correlation suggested by figure 4(c) strongly indicted the temperature-induced fluctuations as the major cause of spot size increase. Discernible graininess in the holographic reconstructions became sharpest in a plane corresponding to the center of the test section. For this reason the optical disturbance was assumed to lie within the test section.

Modulation Transfer Function Tests

The contrast of a sinusoidal image normalized by the contrast of the original object defines the *modulation transfer function* (MTF) of that particular frequency. Reference 3 describes an attempt to quantify the image degradation caused by the flow field with a conventional imaging system and MTF techniques. Figure 5(a) is a sketch of the optical layout for the testing. An image can be thought of as the superposition of optical spatial frequency information analogous to the spectral synthesis of components

in Fourier series. Images are degraded because the higher frequency components, which are essential to synthesize sharp edges, are attenuated. To characterize the effects of phase-altering perturbations, targets of varying frequency are photographed through the disturbance and the contrast is measured. In this particular case a single target having a broad range of frequencies was used as shown in the inset of figure 5(a). Targets were affixed to windows at the four numbered locations. A framing camera with focus fixed at 1 meter was translated to focus consecutively on each of the object planes for steady tunnel conditions. Figures 5(b) and 5(c) summarize the results. Tunnel vibrations limited the usefulness of the tests under flow conditions as shown in figure 5(c). In particular, the image of station 1 was degraded when the fan drive was on, even though the target was outside the flow field. A continuous light source was used and the exposure was controlled by conventional shuttering. Contrast was destroyed at a particular spatial frequency whenever vibration moved the image of an opaque bar into an adjacent clear area during the exposure time.

With the fan off and thus vibration effects eliminated (fig. 5(b)), the results seem to corroborate the results of the holographic tests. Under no-flow conditions the degradation appeared to increase markedly in penetrating the test section. This led to the disturbing conclusion that apparently most of the degradation originated in the test section, but that the degradation was only weakly flow related.

Line Spread Function Tests

Since the MTF tests were hampered by vibrational blurring (within the $\frac{1}{15}$-second exposure times used to record the photographs) and, furthermore, since both MTF and holographic tests were complicated by the presence of an airfoil in the test section, a simple follow-up experiment was designed to verify the earlier results under more straightforward conditions. A very narrow slit was imaged through the flow field and its image recorded. The image of a line source is called the *line spread function* and the modulus of its normalized Fourier transform is the MTF in a direction perpendicular to the imaged slit.

The layout of this experiment is sketched in figure 6. A line source was approximated by forming a 0.127-mm (5-mil) wide slit with razor blades and back-illuminating it with a 75-watt xenon arc lamp run in continuous mode. The reflex camera had a 250-mm focal length lens focused at infinity and operated at $f/5.6$. Exposure times of $\frac{1}{500}$ second resulted in adequate image densities. Figure 7 shows a photograph of the source side pod and figure 8 shows the camera mounted in the receiver pod. Copper tubing

was used to supply purge gas for window defrosting. The optical system provided a geometric image width of 0.026 mm (1 mil) on the film plane. Standard sensitometry techniques were used to interpret negatives read with a Joyce-Loebl scanning microdensitometer. The scanning slit was always at least five times narrower than the geometric image to ensure reasonable fidelity in the recorded data.

Results of the test are summarized in figure 9. The measured widths of the traces at the half-power points were used as a convenient index of the image blurring. The reference width of 0.026 mm (1 mil) recorded under ambient conditions was subtracted from the results to obtain an indicator of the image quality as a function of test conditions. Both flow (fan on) and no-flow (fan off) conditions are plotted. The exposure time may have been inadequate to eliminate vibration effects completely and may explain the difference in the two sets of data. The trend in the data is consistent with that reported in reference 2, and the scale is reasonably accounted for in terms of experimental variables such as focal length, wavelength, and criteria for determining the image blurring. The localization of the disturbance, however, remains uncertain especially in light of the large effect under no-flow conditions.

A test sequel included a dielectric flat mirror mounted on the test section turntable on the source side as shown in figure 10. The mirror redirected the beam back to a beam splitter and into the camera as indicated in the inset. This double-pass scheme eliminated the test section from the optical path. Figure 11 shows the source and camera locations. The beam splitter is obscured by the lamp housing although its support rod is visible. Also shown in the figure is a television camera that was placed to sight through the viewfinder to provide continuous monitoring of the slit image between exposures. The source was operated in a single pulse mode with a pulse duration of 15 microseconds. The reference images obtained with this system were of poorer quality than those obtained in the straight-through slit tests. Under test conditions, in addition to slight asymmetry, some of the images seemed to be modulated with spurious structure. An example is shown in figure 12 taken at 2 atm and 100 K. The dashed addition to the figure represents the more typical profile obtained. Measurements were made only on images that were reasonably symmetric. As with earlier tests the ambient reference width was subtracted. The information was scaled to that of the straight-through tests by dividing by the ratio of the measured pretest image widths for both experiments. The data are plotted as a dashed line in figure 13 along with the data of figure 9 for comparison. These results provided

the first direct evidence that while broadening might still be occurring within the pressure shell, it did not occur inside the test section.

The multipass experiments were extended to include the test section by re-installing the test section windows and placing a second mirror on the far side of the flow field. By shimming the dielectric mirrors and using the parasitic reflections off the windows themselves, it was possible to get simultaneous images resulting from a double pass through the pod only, through the pod and plenum, and through the pod, plenum, and test section. Attempts to obtain quantitative measurements from these data were foiled not only by spurious structure noted in some of the preceding test shots (see fig. 12) but also by the merging and broadening of the multiple images. Thermal contraction of the structure supporting the reflecting optics and/or beam steering due to propagation along non-isothermal paths may have contributed to the image motions. Furthermore, the interpretation of propagating effects over folded paths is complicated by the high correlation present between the incident wave fronts and their retraced counterparts. (See ref. 9.) Regions outside the test section proper were clearly implicated in the image blurring and the correlation with test section parameters, viz., p_t/T_t^2, prompted the design of a temporary facility modification to isolate the plenum and test section effects.

Plenum Isolation Tests

Attempts to sort out the plenum and test section effects using indirect methods were inconclusive. A focused shadowgraph system similar to that sketched in figure 6 was installed with provisions made to penetrate the plenum with cylindrical tubes which could be purged or evacuated as required so that the test section could be viewed directly. It is absolutely essential to provide some means of preventing frost formation on the view ports that separate the cryogenic gas from ambient surroundings. One rugged, reliable method has been to purge the critical window surfaces with dry nitrogen (preferably heated). When this critical surface was the test section window, purge gas had to be supplied through a special insert shown in figure 14. The plenum isolation assembly is shown spanning the plenum region in the top of the figure. The sketch shows an exploded view of the module, which consists of a flange supporting the window which mounts in the test section sidewall, the plenum isolation tube, the inner purge tube, and the coupling flange. Gas flowing between the concentric cylinders flushed the window mounted in the test section wall. The windows are shown mounted in figure 15. To accommodate the

relative motion between the plenum and test section walls, a bellows arrangement was designed into the flange. Although this arrangement possibly induced flow effects, it was unavoidable because of engineering constraints. Measured protrusions into the test section of up to 0.5 mm were noted prior to sealing the test section.

A matrix of test conditions was run with the window and flange in place and the standard 23-cm (9-in.) plenum, or outer pressure shell, windows. The results are shown in figure 16 and are consistent with earlier findings, namely, that the quality of the background optical field degrades as pressure is increased or temperature is decreased. With the purged isolation tubes installed, the optical field improves considerably as shown in figure 17. The curved streak on the photographs was caused by the neutral density filter used for the tests. The ragged appearance around the circumference was apparently due to refraction in the layers of air adjacent to the side tubes. Some graininess in the images is still apparent, especially under the high-pressure or low-temperature conditions. The forced purge required for defrosting unquestionably induces turbulence in the differentially cooled gas. Figure 18 shows the direct comparison between purge-on and purge-off conditions. Note that even the purge-off condition is far from steady state since the gas is expected to settle slowly. It has been standard practice to stop the purge just before taking data. If too much time elapses, the window begins to frost. In the short settling time available, some turbulence is expected to persist.

To completely remove the plenum effects, the purge insert was removed and an extension tube was adapted to the isolation tube so that it would extend into the equipment pod. This component is pictured in figure 19. The small inset figure shows the assembly protruding from the sidewall with the pod removed for clarity. Under these circumstances the isolation tube could be evacuated. The outer window was again purged with dry nitrogen. The results shown in figure 20 indicate that most of the detrimental background "noise" has been removed. While the remaining granularity might be due to the flange not being flush with the sidewall and thus disturbing the flow, it should be noted that some of this appearance persists at 100 K even under no-flow conditions. Results for this series of tests are conveniently summarized in figure 21 which represents the worst test conditions, that is, 5 atm and 100 K. The plenum contributes significantly to the degradation, and plenum isolation cells further improve the quality. Several caustics are evident in the center picture of figure 21. *Caustics* are

concentrations of light corresponding to the envelope of a family of rays and manifest themselves as bright streaks of light. These focusing effects are strikingly similar to those noted in reference 10. Figure 22 juxtaposes two shadowgraphs differing only in the removal of plenum effects. A slight residual graininess remaining in the test-section-only shadowgraph appears to smear in the direction of the flow by an amount consistent with the flow velocity and an exposure duration of 15 microseconds. This is consistent with Taylor's "frozen turbulence" hypothesis which assumes that a given realization of random structure drifts across the measurement aperture with constant velocity determined by local flow conditions but without any other change. (See ref. 11, p. 386.)

As an adjunct to these tests, a number of thermocouples were used to monitor the temperature along the optical paths. The placement of these sensors is indicated in figure 23 along with a sketch to show the locations of optical components. These temperature distributions are time dependent since test conditions in the facility are being changed in ways to minimize tunnel operation costs or to optimize aerodynamic data acquisition. Note that nonisothermal conditions within the plenum, due largely to the thin layer of insulation outside the plenum wall, provide for a flow of heat from the room temperature air surrounding the plenum. Even though the temperature gradients are mild within the plenum and test section, the high pressure and low temperatures encountered there greatly amplify the effects caused by inhomogeneities.

Discussion

In using light beams for optical diagnostics, one tacitly assumes that alterations to the beam take place only in the region under study. Thermal gradients surrounding the test facility, however, can compromise this assumption. While thermal gradients parallel to the beam do not redirect it, gradients transverse to the beam induced by turbulent mixing of regions having different densities can grossly affect the uniformity of the wave front and can alter its direction. Past measurements correlated with total temperature because one boundary condition is the total temperature of the test section while the other is ambient temperature at the far end of the equipment pod. Similarly, the measurements depended on tunnel total pressure in those regions of turbulent mixing within the pressure shell. The increased density in these regions makes them especially critical. Conditions outside the shell are more benign since they remain at ambient pressure, but the mixing is virtually ensured because of normal convection and

especially because of the forced gas purge to maintain frost free windows.

Focusing tests in reference 2, which implicated the test section, may have been insensitive to more subtly distributed inhomogeneities inside and outside the plenum. The structure noted in reference 2 might be related to that shown in the test-section-only photograph in figure 22. This "graininess" persisted in the latest work when the major contributions to beam degradation were removed by evacuating paths leading to and from the test section.

The MTF results described in reference 3 remain puzzling. These data, especially those of figure 5(b), could be explained by a slightly fouled test section window (labeled 2). Subsequent tests confirmed a rather severe oil leak in the tunnel drive train. This was reported in reference 12 and noted in the measurements of reference 13. Oil streaks on models and tunnel walls were noted in the tunnel operation log during the time of these tests. A coating on the test section side of window 2 (see fig. 5(a)) would not affect the target on the plenum side. However, images through this window of targets beyond could be severely degraded. One reason for not questioning the result at the time was that it seemed consistent with the earlier holographic findings. The more subtle effects of the flow may have eluded the sensitivity of the MTF series of experiments.

The line spread function tests corroborated the overall degradation and the double-pass plenum results provided the first clear evidence that a significant part of the problem occurred outside the test section. These experiments provided the impetus for the plenum isolation series. Using a simple shadowgraph field as a visual indicator, it was found that when most of the path subject to temperature gradients was evacuated, the optical quality improved drastically. The isolation tubes extended 60 cm from the centerline. The residual degradation could easily be accounted for by passage through the gradient which contained the flat mirror used to fold the light path and by the expected boundary layer flow turbulence.

Provisions for evacuated paths to and from the test section should be seriously considered in future flow visualization efforts for facilities of this type.

Conclusions and Recommendations

A shadowgraph test has been conducted in the Langley 0.3-Meter Transonic Cryogenic Tunnel which shows that most of the degradation to flow visualization in the facility is not caused by gas within the test section as previously reported. Most of the degradation occurs outside the test section between

the test section wall and the pressure shell where temperature gradients can induce inhomogeneities in the refractive index. The effects of these inhomogeneities in the plenum are increased by high pressure (p) and low temperature (T) with a p/T^2 dependence. Provisions for evacuated paths to and from the test section should be seriously considered in future flow visualization efforts for facilities of this type.

NASA Langley Research Center
Hampton, VA 23665-5225
June 10, 1986

References

1. McKinney, L. Wayne; and Baals, Donald D., eds.: *High Reynolds Number Research—1980.* NASA CP-2183, 1981.

2. Burner, A. W.; and Goad, W. K.: *Flow Visualization in a Cryogenic Wind Tunnel Using Holography.* NASA TM-84556, 1982.

3. Snow, W. L.; Burner, A. W.; and Goad, W. K.: *Image Degradation in Langley 0.3-Meter Transonic Cryogenic Tunnel.* NASA TM-84550, 1982.

4. Rhodes, D. B.; and Jones, S. B.: Flow Visualization in the Langley 0.3-Meter Transonic Cryogenic Tunnel and Preliminary Plans for the National Transonic Facility. *Flow Visualization and Laser Velocimetry for Wind Tunnels,* NASA CP-2243, 1982, pp. 117–132.

5. Ray, Edward J.; Ladson, Charles L.; Adcock, Jerry B.; Lawing, Pierce L.; and Hall, Robert M.: *Review of Design and Operational Characteristics of the 0.3-Meter Transonic Cryogenic Tunnel.* NASA TM-80123, 1979.

6. Tatarsky, V. I. (R. A. Silverman, transl.): *Wave Propagation in a Turbulent Medium.* McGraw-Hill Book Co., Inc., 1961.

7. Uscinski, B. J.: *The Elements of Wave Propagation in Random Media.* McGraw-Hill International Book Co., c.1977.

8. Hufnagel, Robert E.: Propagation Through Atmospheric Turbulence. *The Infrared Handbook,* William L. Wolfe and George J. Zissis, eds., Office of Naval Research, Department of the Navy, 1978, pp. 6-1–6-56.

9. Smith, Jack; and Pries, Thomas H.: Temporal-Frequency Spectra for Waves Propagating Over Straight and Folded Paths: A Comparison. *Appl. Opt.,* vol. 14, no. 5, May 1975, pp. 1161–1164.

10. Parry, G.; Pusey, P. N.; Jakeman, E.; and McWhirter, J. G.: Focussing by a Random Phase Screen. *Opt. Commun.,* vol. 22, no. 2, Aug. 1977, pp. 195–201.

11. Goodman, Joseph K.: *Statistical Optics.* John Wiley & Sons, Inc., c.1985.

12. Honaker, William C.; and Lawing, Pierce L.: *Measurements in the Flow Field of a Cylinder With a Laser Transit Anemometer and a Drag Rake in the Langley 0.3 m Transonic Cryogenic Tunnel.* NASA TM-86399, 1985.

13. Hall, Robert M.: Pre-Existing Seed Particles and the Onset of Condensation in Cryogenic Wind Tunnels. AIAA-84-0244, Jan. 1984.
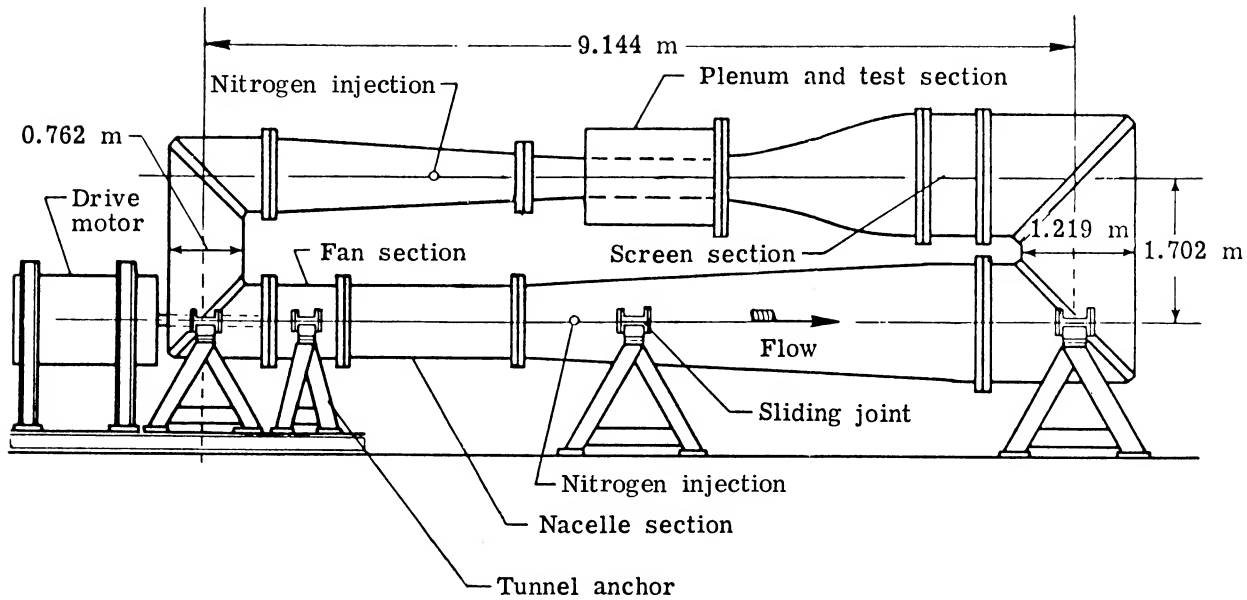
Figure 1. Schematic of Langley 0.3-Meter Transonic Cryogenic Tunnel.
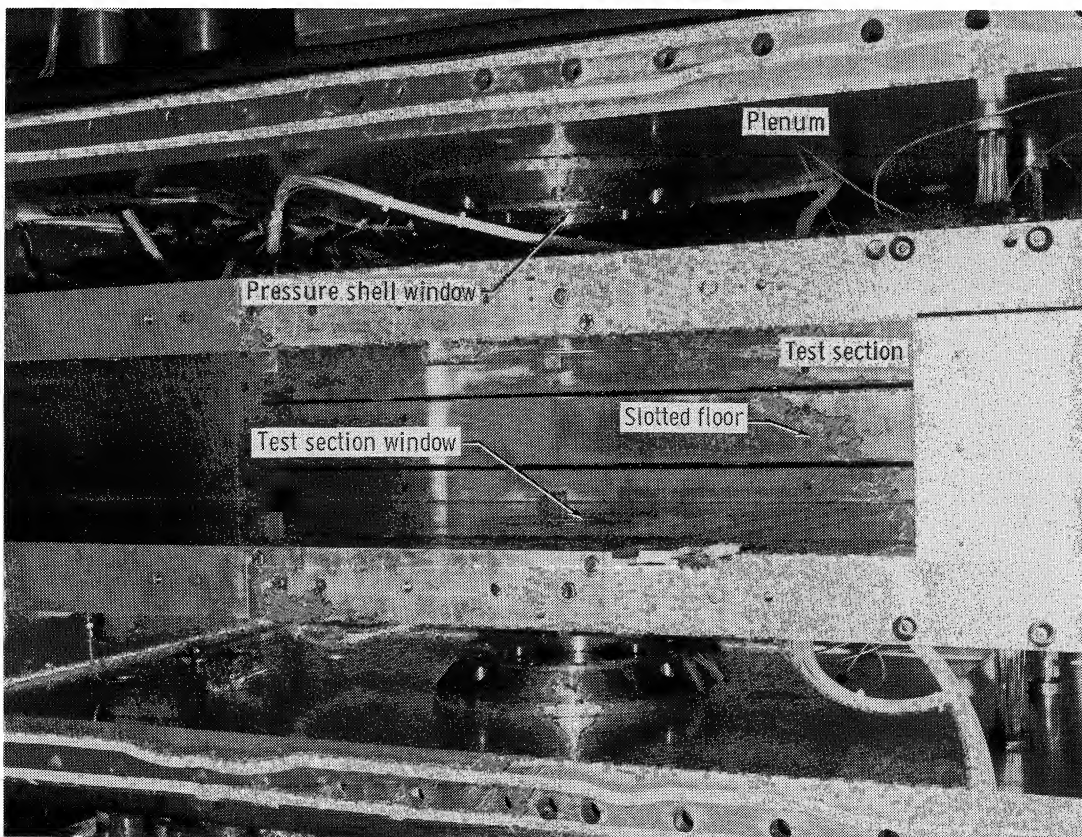
L-84-2939

Figure 2. Top view of test section and plenum with cover plate removed.
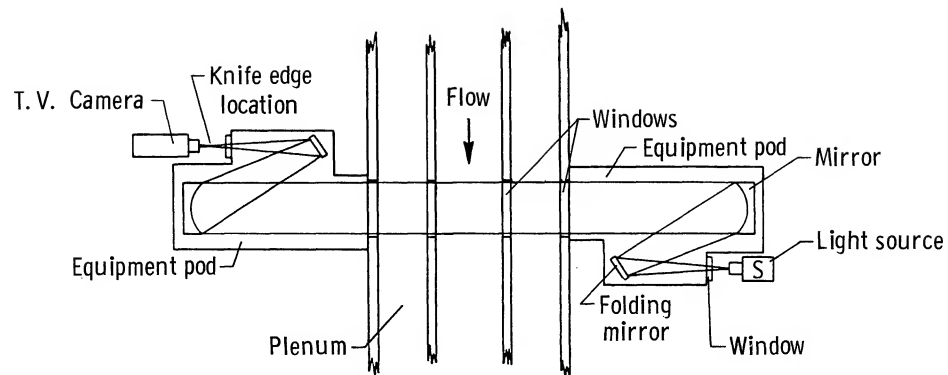
Figure 3. Top view schematic showing relationship of equipment pods to the wind tunnel.
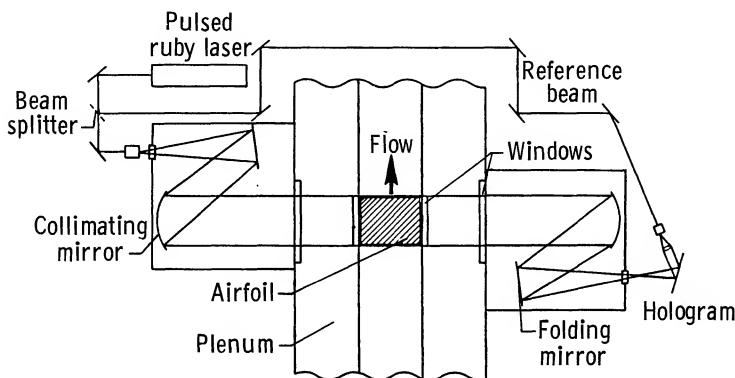
(a) Optical layout (top view).
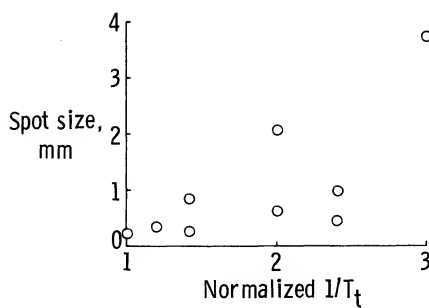
(b) Spot size of reconstructed images plotted against $1/T_t$.
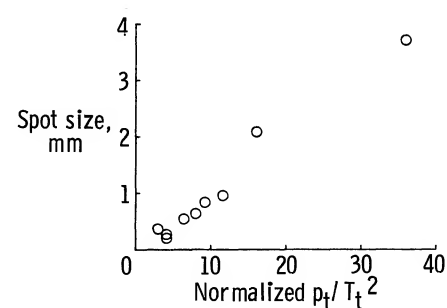
(c) Spot size of reconstructed images plotted against p_t/T_t^2.

Figure 4. Configuration and results of holographic experiment described in reference 2.
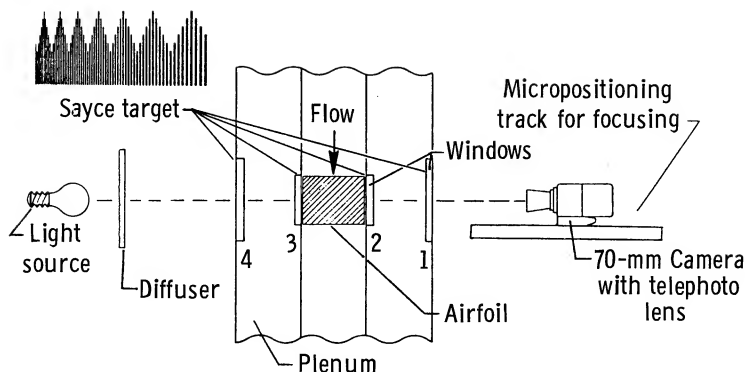
(a) Optical layout.
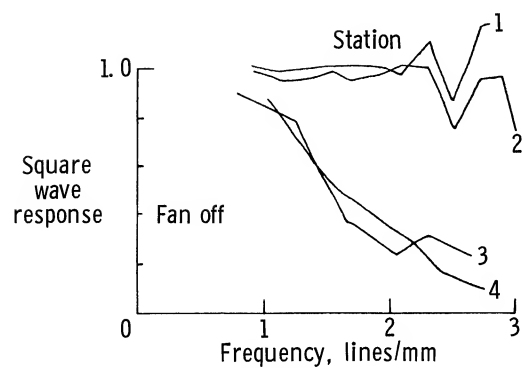
(b) Fan off.
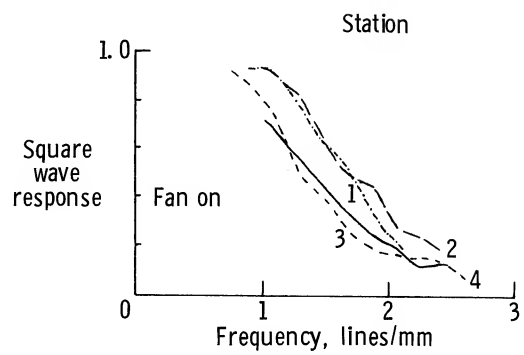
(c) Fan on.

Figure 5. Configuration and test results for 120 K and 5 atm described in reference 3.
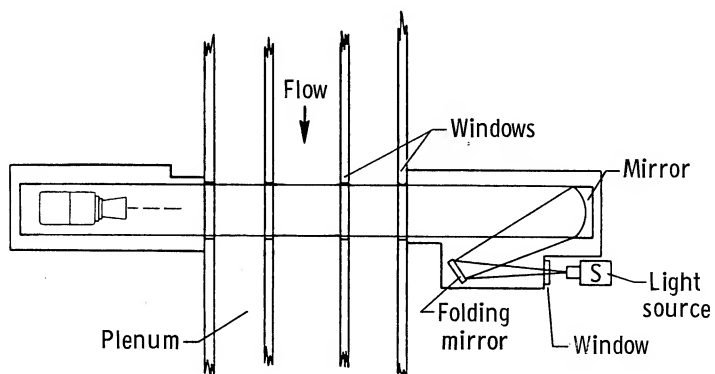
Figure 6. Experimental layout (top view) for straight-through slit tests.
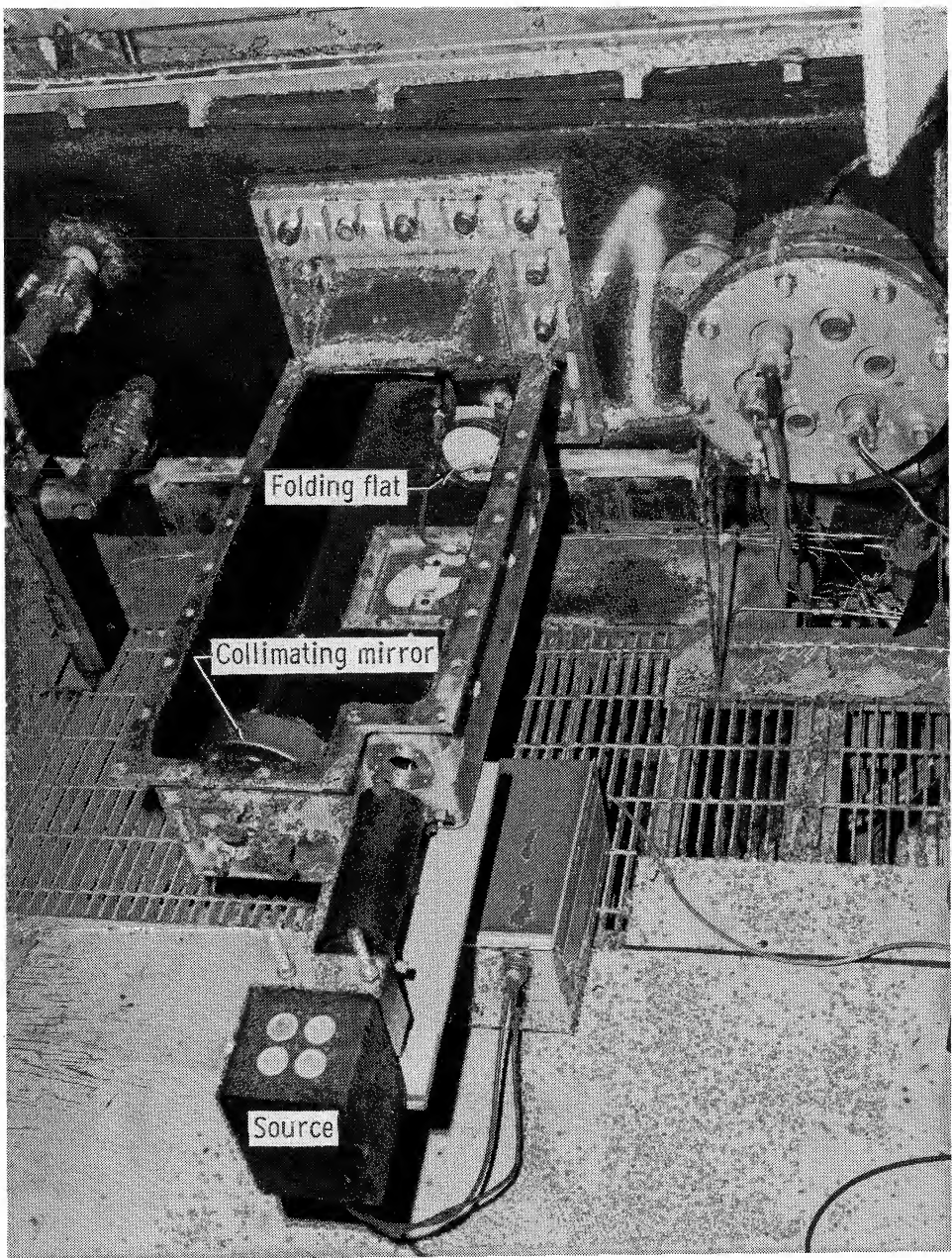
Figure 7. Equipment pod, attached to tunnel sidewall, used for source during straight-through slit tests.
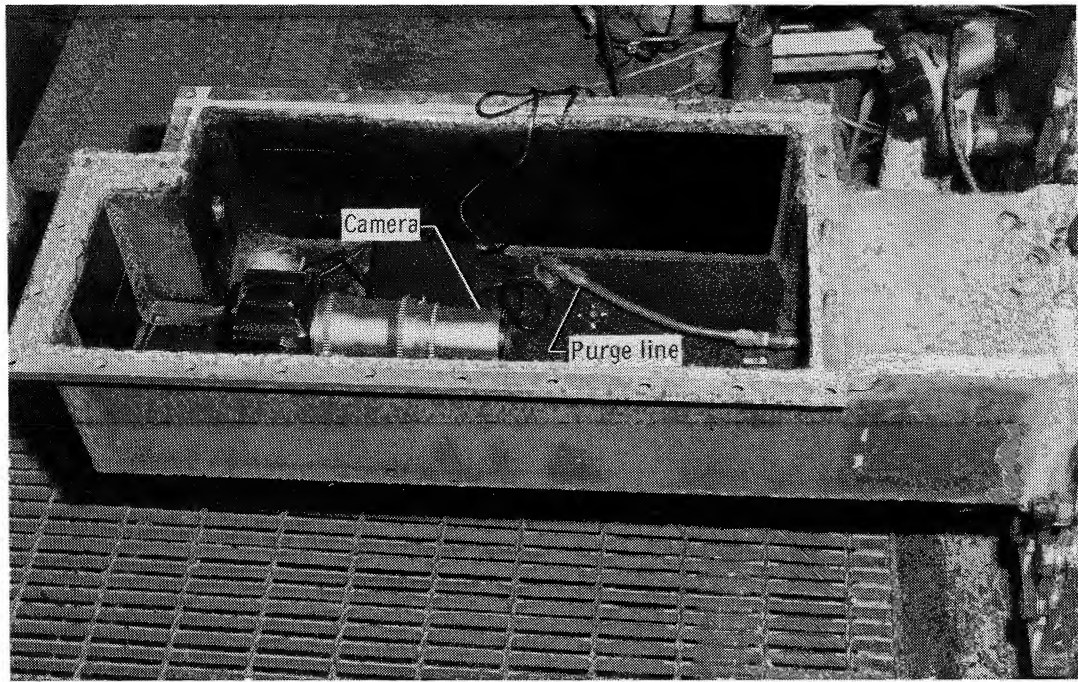
L-84-2941

Figure 8. Equipment pod used for receiving optics during straight-through slit tests.
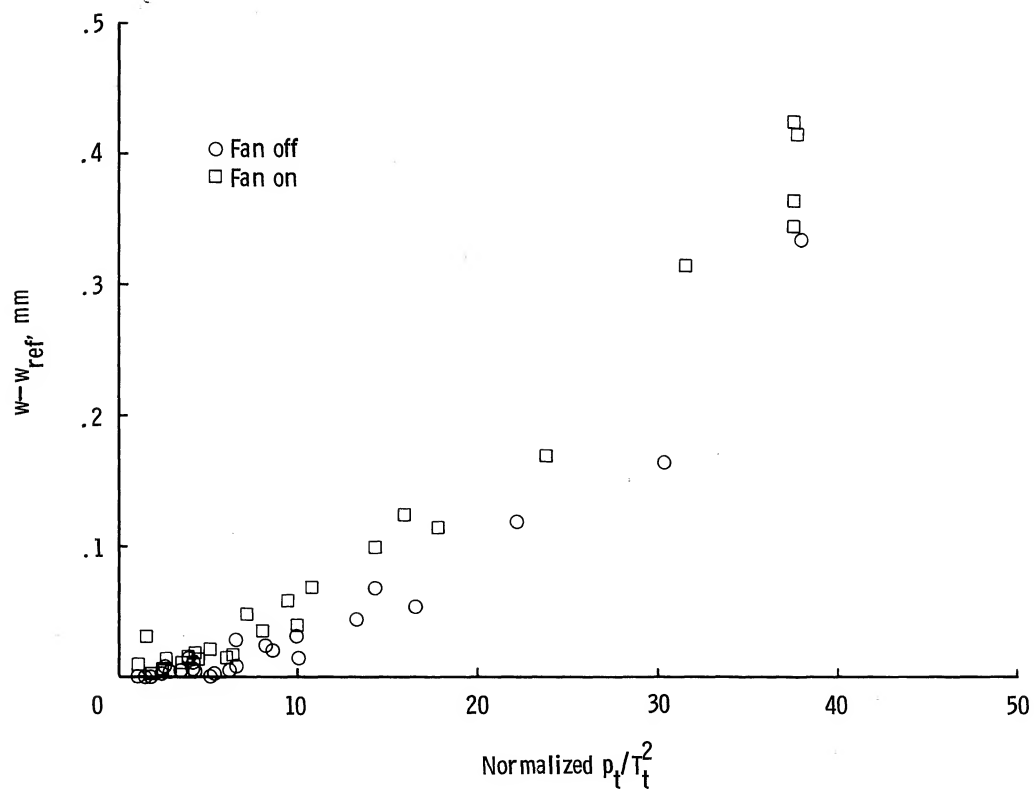
Figure 9. Plot of apparent width of slit image versus p_t/T_t^2 for straight-through slit tests.

11
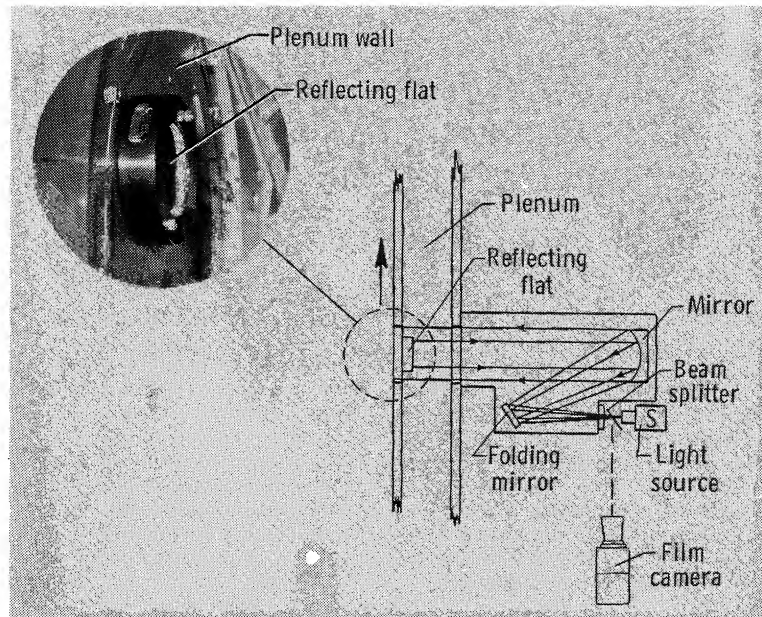
Figure 10. Optical layout for double-pass experiment eliminating the test section from the optical path. The inset shows the reflecting mirror mounted for the test.
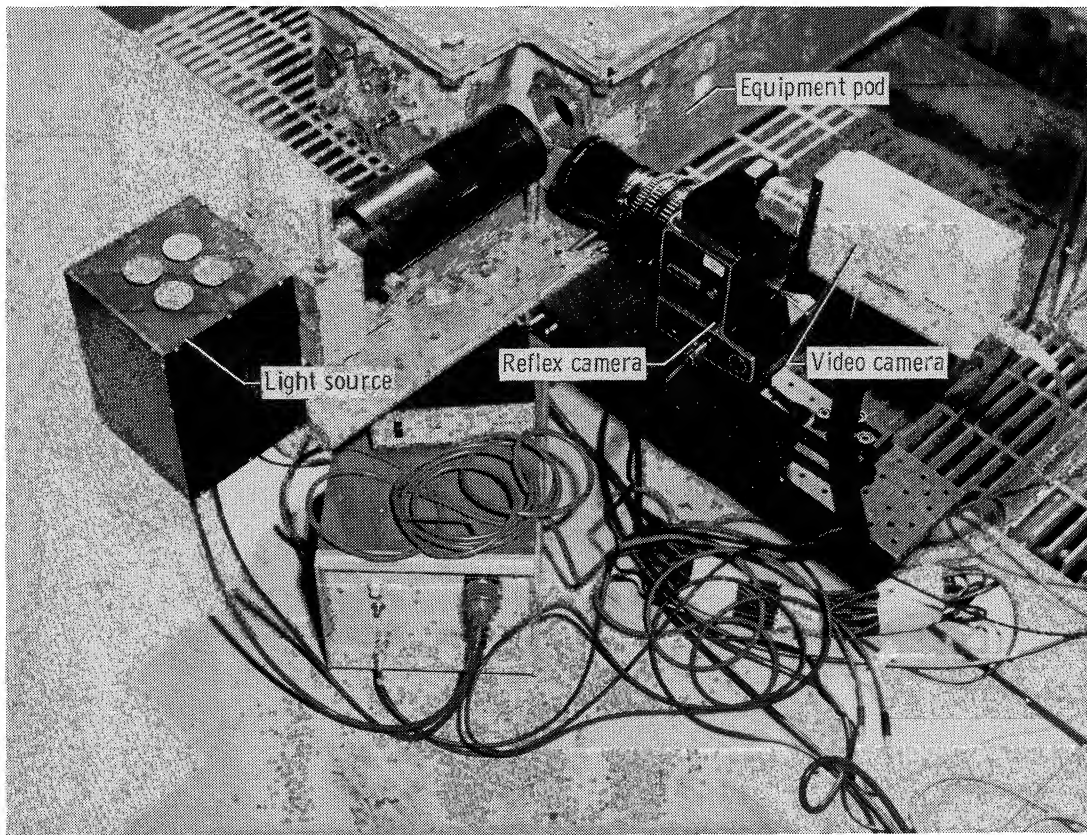
L-83-2803

Figure 11. Experimental arrangement for double-pass experiment showing the pulsed light source, reflex camera, and video camera locations.
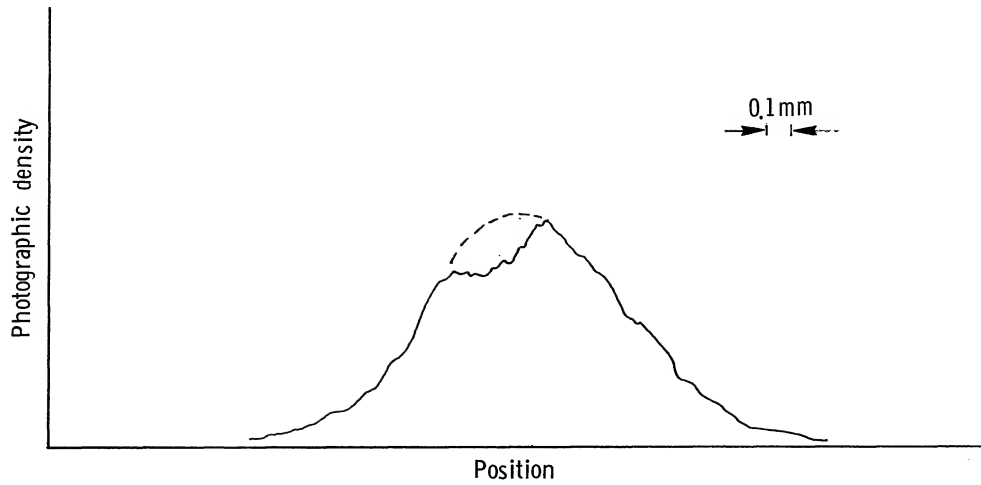
Figure 12. Densitometer trace of a questionable exposure of a slit imaged through the plenum using the double-pass arrangement. Subsequent exposures under the same tunnel conditions resulted in traces having better symmetry about the vertical centerline (dashed).
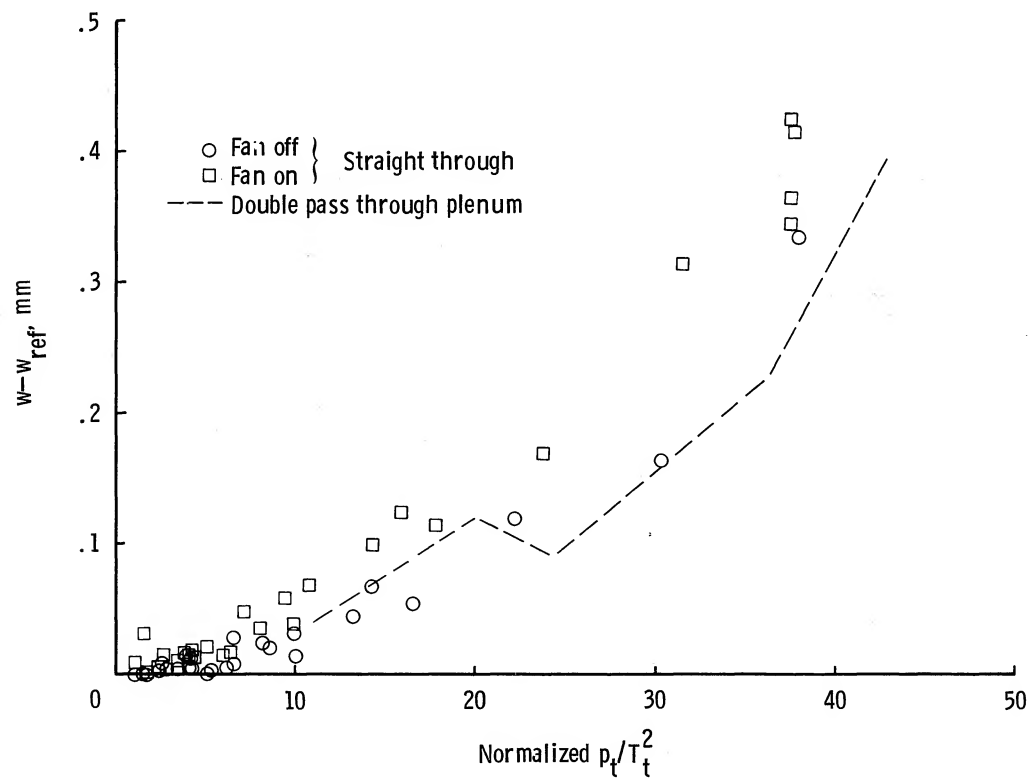
Figure 13. Plot of apparent width of slit image versus p_t/T_t^2 for straight-through and double-pass slit tests.
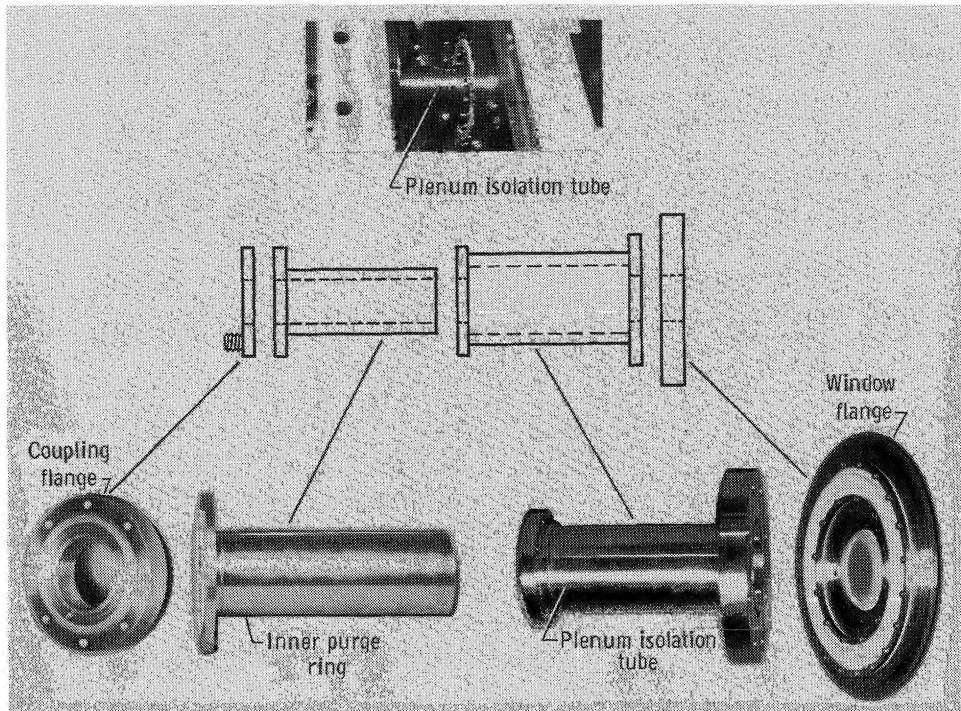
Figure 14. Plenum isolation assembly. The telescoping center components are designed to allow purging of the window with dry nitrogen. The assembled tube is shown mounted in the facility in the inset.
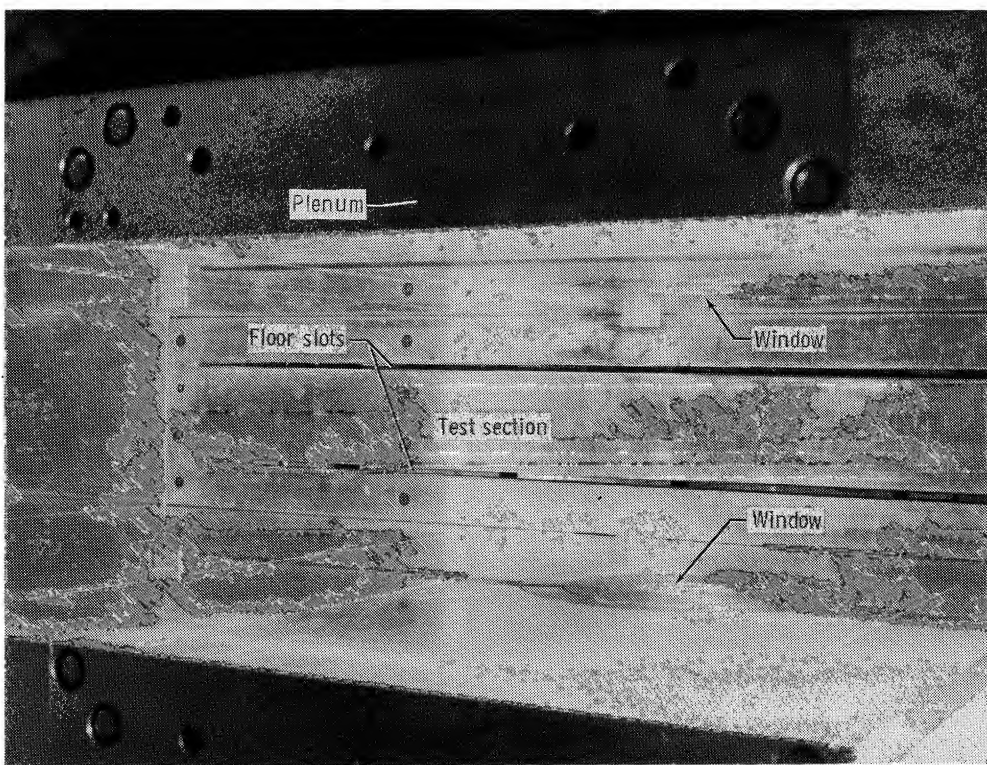
L-84-2938

Figure 15. Top view of test section showing slotted floor. Sidewall windows are visible in the photograph.
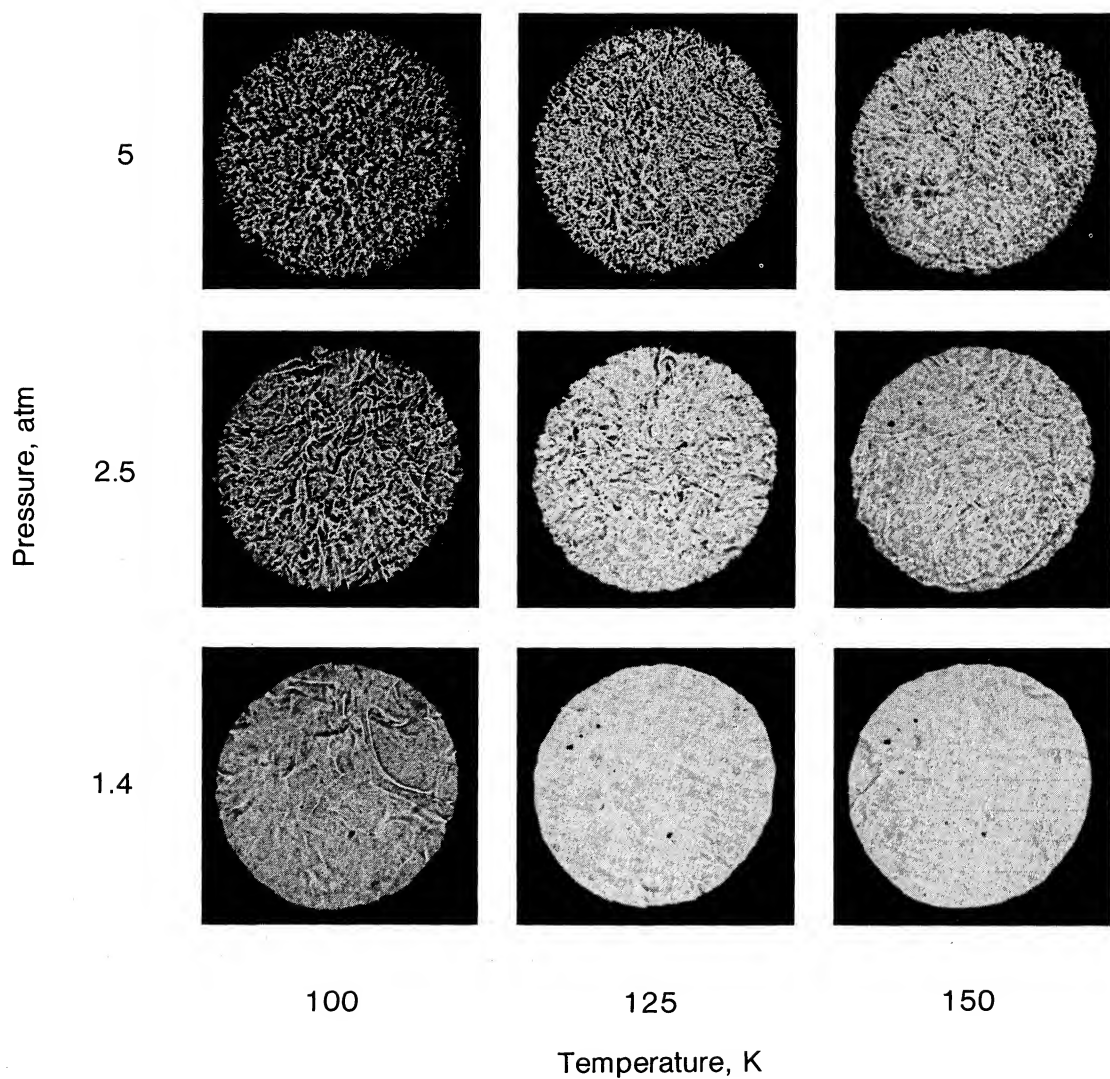
Figure 16. Representative sample of shadowgraph background quality as a function of test conditions. The shadowgraph is focused at the center of test section. The optical path includes both test section and plenum. Mach 0.65.
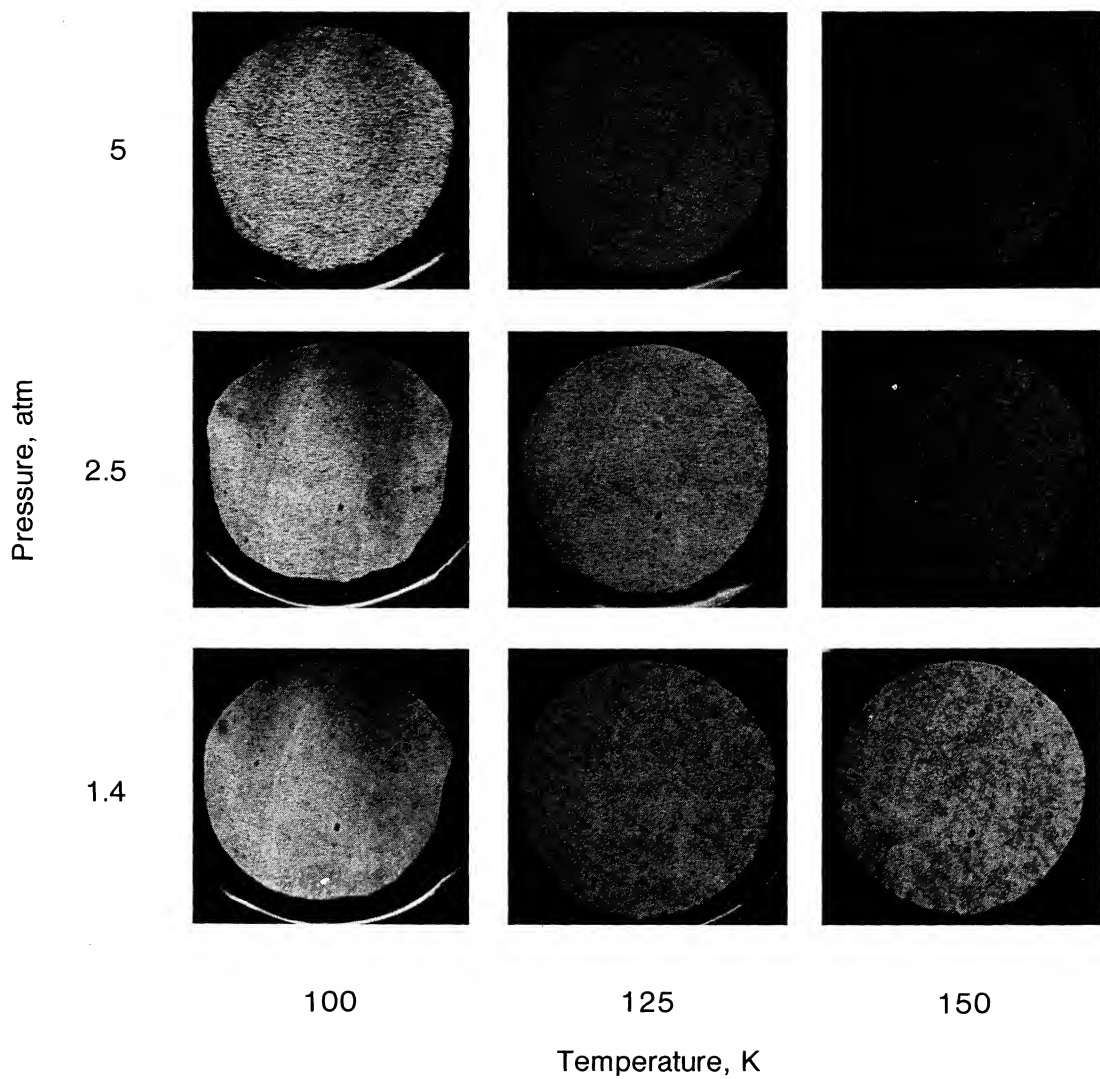
Figure 17. Shadowgraph focused at the center of the empty test section with purged cell replacing the plenum part of the optical path. Mach 0.65.
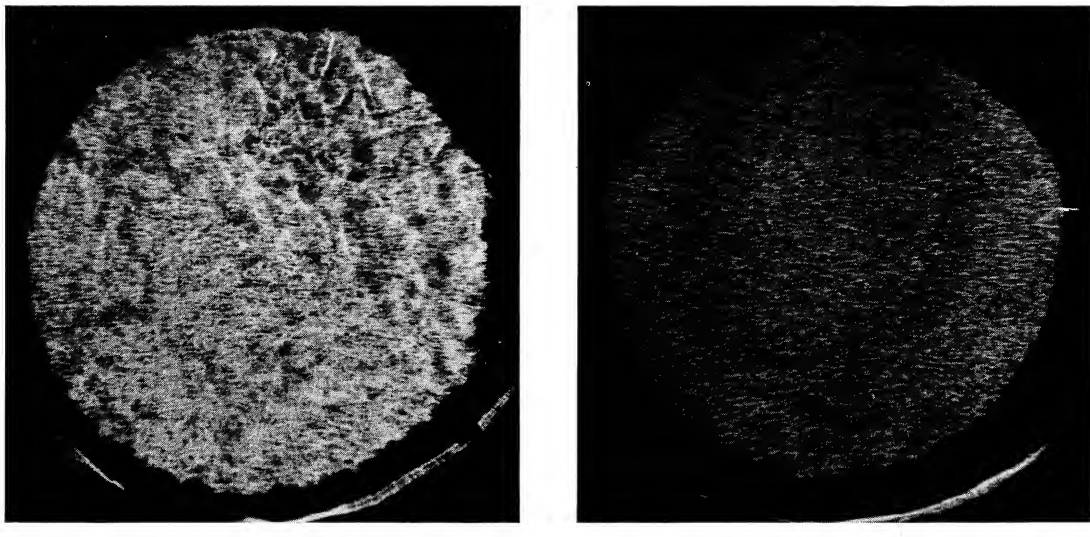
Purge on   Purge off

Figure 18. Purge gas effect on focused shadowgraph images. Optical path includes test section and purged cell. $T_t = 100$ K; $p_t = 5$ atm; Mach 0.65.
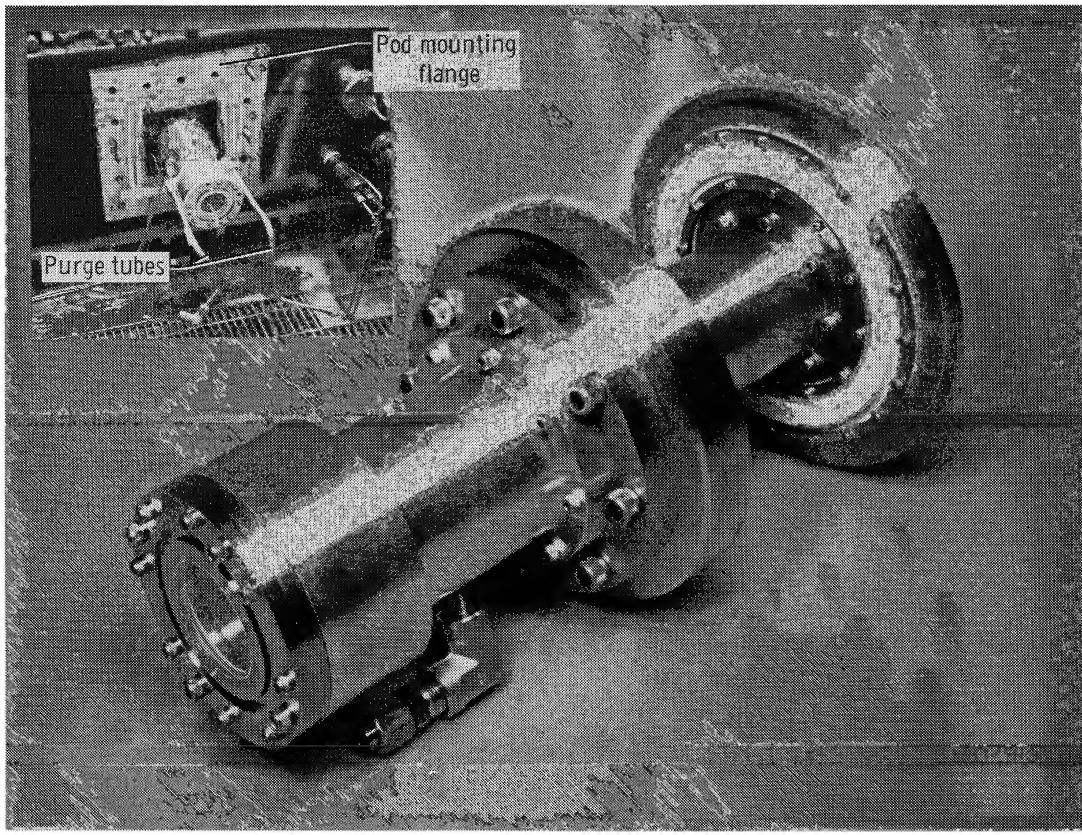
L-84-2262

Figure 19. Plenum isolation tube with one extension section. Fully assembled tube shown mounted on the facility with pod removed. Tubing used to evacuate the assembly is visible.
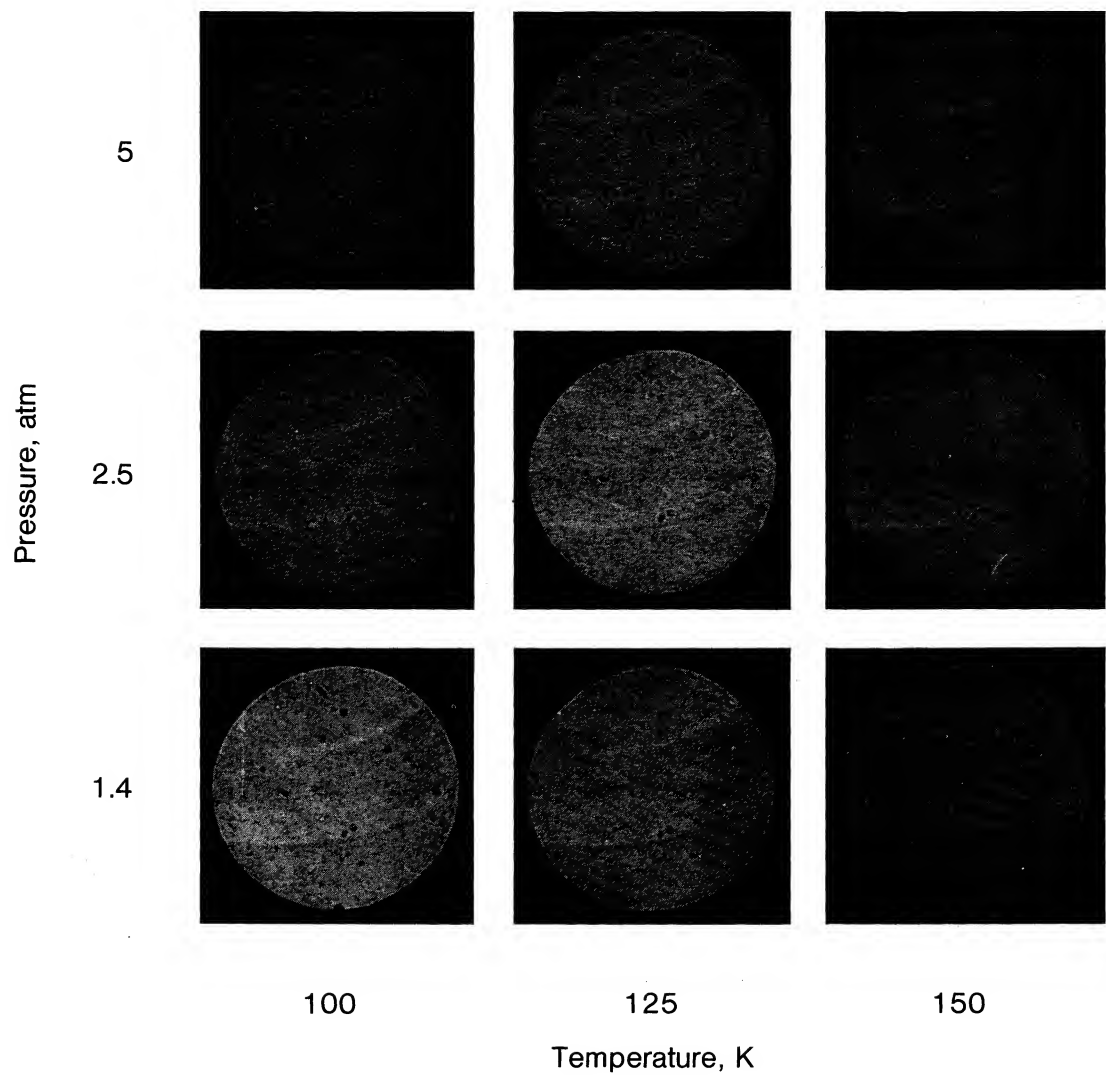
Figure 20. Shadowgraph results with evacuated paths leading to and from the test section for a matrix of test conditions. Shadowgraph focused on center of empty test section. Mach 0.65.
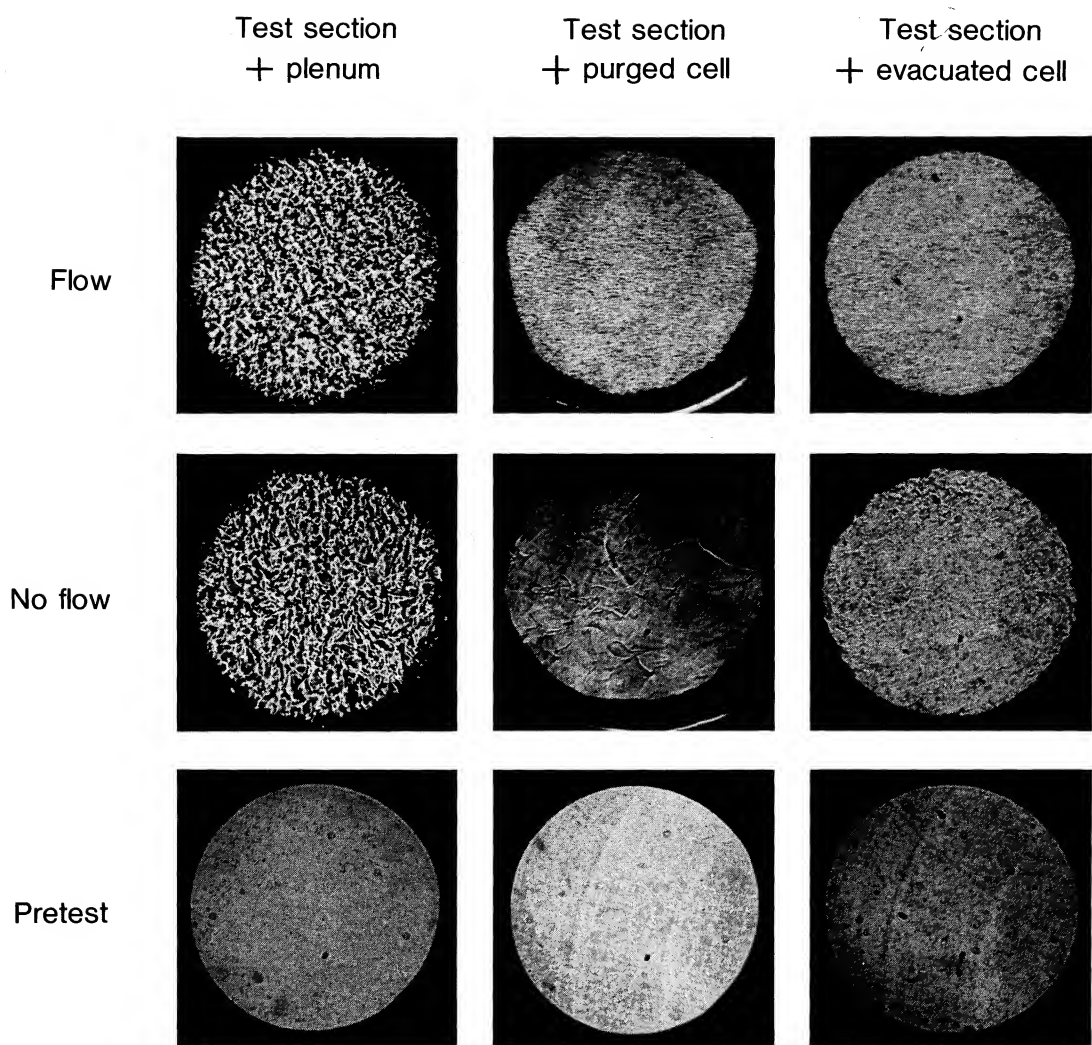
Figure 21. Synopsis of results under flow and no-flow conditions showing the effects of isolating the plenum (center column) and evacuating the path to and from the test section (right column). $p_t = 5$ atm; $T_t = 100$ K; Mach 0.65.
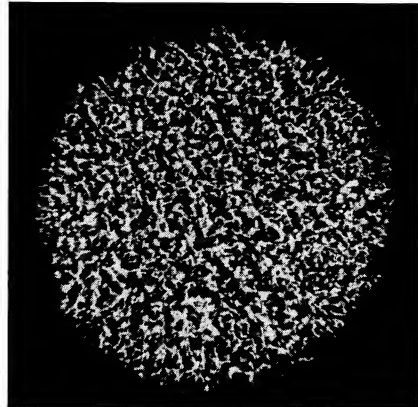
Test section + plenum   Test section only
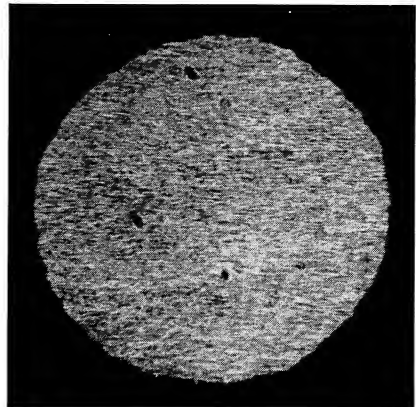
Figure 22. Shadowgraphs taken without (left) and with (right) evacuation of path leading to the test section. $T_t = 100$ K; $p_t = 5$ atm; Mach 0.65.
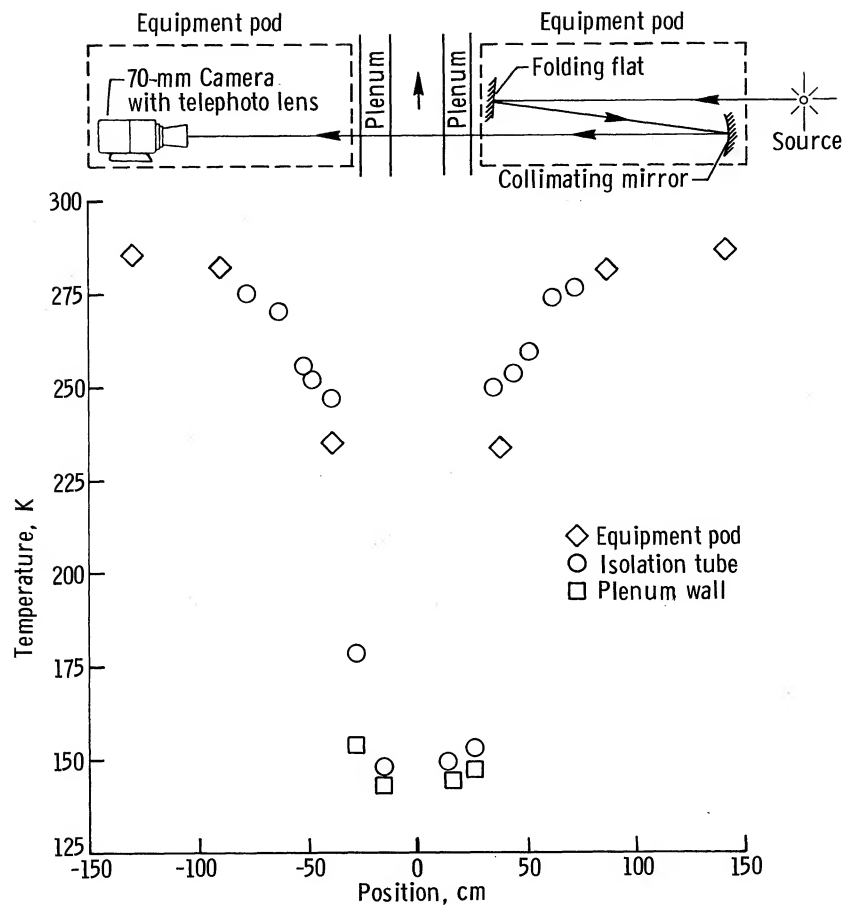
Figure 23. Measured temperature distribution along the direction of optical propagation and transverse to the flow. The sketch at the top is scaled to the horizontal (optical) axis.

Standard Bibliographic Page

1. Report No. NASA TM-87730	2. Government Accession No.	3. Recipient's Catalog No.
4. Title and Subtitle Improvement in the Quality of Flow Visualization in the Langley 0.3-Meter Transonic Cryogenic Tunnel		5. Report Date August 1986
		6. Performing Organization Code 505-61-01-05
7. Author(s) Walter L. Snow, Alpheus W. Burner, and William K. Goad		8. Performing Organization Report No. L-16108
9. Performing Organization Name and Address NASA Langley Research Center Hampton, VA 23665-5225		10. Work Unit No.
		11. Contract or Grant No.
12. Sponsoring Agency Name and Address National Aeronautics and Space Administration Washington, D.C. 20546-0001		13. Type of Report and Period Covered Technical Memorandum
		14. Sponsoring Agency Code

15. Supplementary Notes

16. Abstract

Optical diagnostic techniques have not been as successful in the 0.3-Meter Transonic Cryogenic Tunnel as in conventional wind tunnels. This paper describes a simple shadowgraph experiment which allowed evacuation of the optical paths outside the test section. The results of this study show that refractive index variations induced by temperature gradients outside the test section account for most of the image degradation. Earlier reports had erroneously attributed this degradation to inhomogeneities in the test section. Evacuation of the paths leading to and from the test section significantly improves the quality of flow visualization.

17. Key Words (Suggested by Authors(s)) Langley 0.3-Meter Transonic Cryogenic Tunnel Flow visualization Shadowgraph Thermal gradients Plenum effects	18. Distribution Statement Unclassified—Unlimited Subject Category 35		
19. Security Classif.(of this report) Unclassified	20. Security Classif.(of this page) Unclassified	21. No. of Pages 22	22. Price A02